BULLETIN OF THE POLISH ACADEMY OF SCIENCES
TECHNICAL SCIENCES, Vol. 73(4), 2025, Article number: e154277
DOI: 10.24425/bpasts.2025.154277

MECHANICAL AND AERONAUTICAL ENGINEERING, THERMODYNAMICS

Design and implementation of non-circular gears based on target transmission ratio

Weizhen SONG and Yong HE*

School of Mechanical Engineering, Donghua University, Shanghai, 201620, China

Abstract. Addressing the complexities inherent in current specific non-circular gear design, including the extensive computational demands involved in solving tooth profile feature points and the lack of a rigorous design and verification process, this study proposes a design method grounded in gear meshing theory. Specifically, the method focuses on achieving the target transmission ratio for non-circular gear. First, the pitch curve equation for the non-circular gear is computed. Secondly, an equal arc length algorithm is proposed to determine the polar diameter rotation angle corresponding to the same arc length per turn, generating a non-circular gear envelope diagram using the equal arc length enveloping method. Subsequently, an edge extraction algorithm is presented to obtain the tooth profile feature data. After obtaining tooth profile feature data, the 3D model of non-circular gears is generated. Then, the gear pair is virtually assembled, and the meshing process is analyzed using a motion simulation method. The results show that the tooth profile meshes well, and the angular velocity curve of the driven wheel is consistent with the target transmission ratio. Finally, the processed non-circular gear was inspected, and the results indicated that the error between the produced non-circular gear and the theoretical tooth profile was within a reasonable range. This confirms the accuracy of the proposed method and provides a rigorous design and verification process for non-circular gears, which is beneficial for further analysis in manufacturing and other tasks. This method not only significantly reduces computation time but also simplifies the process of extracting tooth profile feature points, ensuring extraction accuracy.

Keywords: non-circular gear; target transmission ratio; kinematic analysis; tooth profile extraction; equal arc length algorithm.

1. INTRODUCTION

Non-circular gears can achieve variable-speed transmission between two mechanisms, making them superior transmission components with successful applications in light industry machinery [1], rice machinery [2], and other fields [3–5]. Due to their unique ability to achieve variable transmission ratios, they can precisely control the output speed in numerous practical applications. However, typical non-circular gears struggle to meet particular transmission requirements, necessitating designs based on target transmission ratios.

Designing non-circular gears has been widely researched. Jang Hyo-Seong *et al.* [6] deduced the pitch curve based on the required angular speed ratio and conducted a dynamic analysis based on the pitch curve, yet it does not involve processing the actual dimensions. Silvia Maláková *et al.* [7] designed an eccentric gear pair with a transmission ratio ranging from 0.5 to 2, but the design process is cumbersome, overly reliant on 2D design software, and lacks profile extraction, making the overall design process difficult to understand. Liu Dawei *et al.* [8] used non-circular gears to simulate limacon gears, optimizing without solving the process according to the pitch curve, but without conducting a kinematic analysis of the obtained gear. Figliolini [9] analyzed non-circular gear pairs focusing on pressure angle, pitch curve, and convex-concave characteristics, but did not create 2D or 3D models of non-circular gears. Liu Youyu *et al.* [10] designed elliptical gear pairs and explained the design process, but did not conduct kinematic analysis to verify its correctness. The analysis of published research reveals the following issues: Most non-circular gear tooth profile designs [6–8] rely on 2D or 3D design software, which is expensive, and its accuracy cannot be guaranteed. In some articles [5, 6, 8, 11], the number of teeth and modules is set first, followed by the calculation of undercutting, which leads to an incorrect overall solution sequence. In some articles [3, 5], the process of extracting non-circular gear tooth profiles is complex, with a large computational load, making it difficult to reproduce, and even resulting in the loss of some tooth profile points. This paper addresses these issues by providing a comprehensive design and validation process for non-circular gears, which serve as a reference for high-precision design and manufacturing.

This paper covers the following research: first, solving the pitch curve based on the transmission ratio. Next, an equal arc length method is proposed, which does not require extensive calculations. Then, the equal arc length envelope method is used to generate the envelope diagram of the non-circular gear and to extract tooth profile feature points. Finally, the assembled model is imported for kinematic analysis.

*e-mail: heyong@dhu.edu.cn

Manuscript submitted 2025-01-13, revised 2025-03-22, initially accepted for publication 2025-04-07, published in July 2025.

2. BASIC THEORY

2.1. Transmission ratio

The gear transmission ratio [12] is a function of the driving wheel angle, serving as the independent variable. For an external gear pair, as shown in Fig. 1, the transmission ratio [13] is $i_{12}(\varphi_1) = f(\varphi_1)$ can be inferred from the following motion law

$$i_{12} = \frac{r_2}{r_1} = \frac{\mathrm{d}\varphi_1}{\mathrm{d}\varphi_2} = \frac{\omega_1}{\omega_2}, \tag{1}$$

where ω_1 and ω_2 are the angular speeds of the driving and driven gears, respectively.

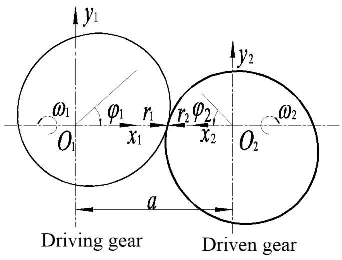

Fig. 1. Non-circular gears meshing transmission

2.2. Pitch curve and arc length

Assuming that the center distance is a, the transmission ratio is $i_{12} = f(\varphi_1)$, then get the driving wheel pitch curve

$$r_1(\varphi_1) = \frac{a}{1 + f(\varphi_1)}. \tag{2}$$

The pitch curve equation $r_2(\varphi_1)$ of the driven wheel is

$$r_2(\varphi_1) = a - r_1(\varphi_1) = \frac{a f(\varphi_1)}{1 + f(\varphi_1)}, \tag{3}$$

$$\varphi_2 = \int_0^{\varphi_1} \frac{1}{f(\varphi_1)} \mathrm{d}\varphi_1. \tag{4}$$

In Cartesian coordinates, the equations of the driving and driven wheel pitch curve are

$$\begin{aligned} x_1 &= r_1 \sin(\varphi_1), \\ y_1 &= r_1 \cos(\varphi_1), \end{aligned} \tag{5}$$

$$\begin{aligned} x_2 &= r_2 \cos\left(\varphi_2 - \frac{\pi}{2}\right), \\ y_2 &= r_2 \sin\left(\varphi_2 - \frac{\pi}{2}\right) + a. \end{aligned} \tag{6}$$

Given that the gear pair is capable of achieving full rotation, the motion process can be equated to pure rolling. The length of the pitch curve [14] is calculated as follows:

$$L = \int_0^{2\pi} \sqrt{r_1^2(\varphi_1) + r_1'^2(\varphi_1)}\, \mathrm{d}\varphi_1 = \int_0^{2\pi} f_1(\varphi_1)\, \mathrm{d}\varphi_1. \tag{7}$$

2.3. Radius of curvature

The radius of curvature is computed using a numerical method outlined in reference [8].

Figure 2 illustrates a circular arc. Three points A, B, and C on the pitch curve are selected arbitrarily. The coordinates of these points are (x_i, y_i), (x_{i+1}, y_{i+1}), (x_{i+2}, y_{i+2}). When A, B, and C are sufficiently close, the length of OA approximates the curvature radius of the arc segment ABC. Let the coordinates of O be (x, y), and the slope of line Oa is k_1, the slope of line Ob is k_2, the curvature radius of arc length ABC is ρ, then we obtain

$$k_1 = \frac{x_{i+1} - x_i}{y_{i+1} - y_i}, \tag{8}$$

$$k_2 = \frac{x_{i+2} - x_{i+1}}{y_{i+2} - y_{i+1}}, \tag{9}$$

$$y - \frac{y_i + y_{i+1}}{2} = k_1\left(x - \frac{x_i + x_{i+1}}{2}\right), \tag{10}$$

$$y - \frac{y_{i+1} + y_{i+2}}{2} = k_2\left(x - \frac{x_{i+1} + x_{i+2}}{2}\right), \tag{11}$$

$$\rho = \sqrt{(x - x_i)^2 + (y - y_i)^2}. \tag{12}$$

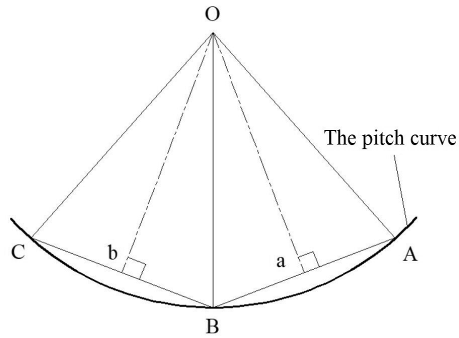

Fig. 2. Curvature radius of pitch curve

2.4. Gear undercut

Due to the unique profile of non-circular gears, the curvature radius at each position varies. Consequently, the gear undercut phenomenon may occur during machining [11], most likely at locations where the curvature radius is minimal. Thus, it is essential to verify the potential for gear undercut. When employing a rack cutter to machine non-circular gears, the condition to avoid gear undercut is represented by

$$h_{a0}^* m \le \rho_{\min} \sin^2 \alpha_0, \tag{13}$$

where $\rho_{\min}$ denotes the minimum curvature radius, α_0 typically equals $\alpha_0 = 20°$, and h_{a0}^* signifies addendum coefficient, usually $h_{a0}^* = 1$. Utilizing equation (13), the modulus range ensuring no gear undercut can be determined

$$m_{\max} \le \frac{\rho_{\min} \sin^2 \alpha_0}{h_{a0}^*}, \tag{14}$$

$$z_{\min} = \frac{L}{\pi m_{\max}}. \tag{15}$$

3. EXAMPLE ANALYSIS AND SOLUTION

3.1. Example analysis

Assuming the center distance is set at 48.17 mm and the target transmission ratio is $i_{12}(\varphi_1) = 1.118 + 0.5\sin(\varphi_1)$, by applying formulas (2) and (3), the pitch curves for the driving and driven wheels can be calculated

$$r_1(\varphi_1) = \frac{48.17}{2.118 + 0.5 \times \sin(\varphi_1)}, \tag{16}$$

$$r_2(\varphi_1) = \frac{48.17 \times (1.118 + 0.5 \times \sin(\varphi_1))}{2.118 + 0.5 \times \sin(\varphi_1)}. \tag{17}$$

According to formula (7), the driving wheel pitch curve is derived

$$L = \int_0^{2\pi} \sqrt{r_1^2(\varphi_1) + \left(\frac{\mathrm{d}r_1(\varphi_1)}{\mathrm{d}\varphi_1}\right)^2}\, \mathrm{d}\varphi = 149.2. \tag{18}$$

The arc length of the driving wheel is 149.2 mm. Figure 3 shows the arc length of the integral function L and rotation angle φ_1 of the driving gear.

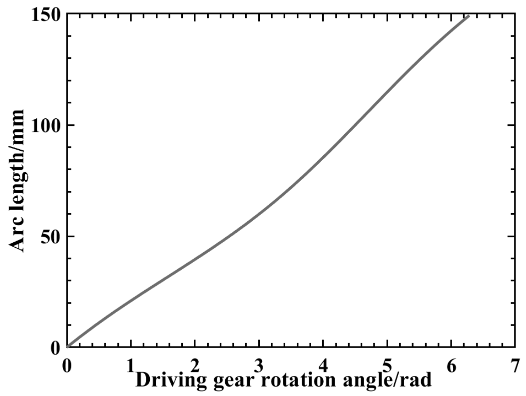

Fig. 3. The angle and arc length

The pitch curves of the driving and driven gears in Fig. 4 can be obtained by solving the equations (5), (6), (16), and (17). Figure 4 shows the initial rotation position.

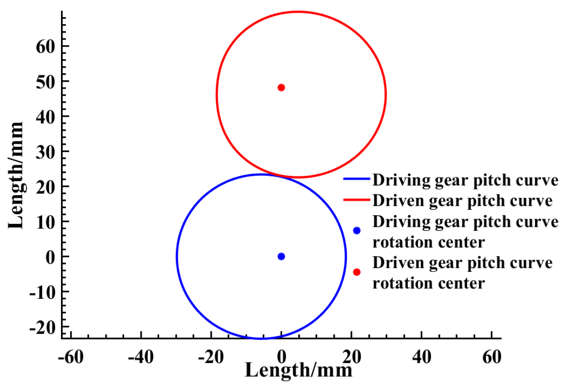

Fig. 4. Non-circular gear pitch curve

Following formulas (16) (17), and substituting into formula (12), the minimum curvature radius for the driving and driven wheels are $\rho_{1\,\min} = 22.743$ and $\rho_{2\,\min} = 22.187$. To ensure no gear undercut occurs during the involvement of gear machining, the conditions in formula (13) should be satisfied. $\rho_{1\,\min}$ and $\rho_{2\,\min}$ entered into formula (14), the modules of the driving and driven wheel $m_{1\,\max} \le 2.66$ and $m_{2\,\max} \le 2.595$ are obtained. According to formula (15), we obtain the minimum number of teeth $z_{1\,\min} = 17.851$ and $z_{2\,\min} = 18.298$. To align non-circular gears with standard gear design practices, common module sizes are typically selected. Therefore, this study opts for a module of 2.5, and a tooth chosen to count 19 to satisfy design requirements.

This paper specifies a non-circular gear module m of 2.5 mm, with both the driving and driven wheels featuring 19 teeth. The paper [7] outlines the steps in the design process:

1. Determine the center distance and target transmission ratio.
2. Solve the pitch curve equations.
3. Determine the minimum curvature radius, the maximum modulus, and the minimum number of teeth. Determine the number of teeth and modulus for both the driving and driven wheels.
4. Verify whether the number of teeth and modulus align with design requirements, if yes, turn 5; otherwise, turn 3.
5. Draw a non-circular wheel pitch curve. End.

3.2. Rotation center and gear shaper cutter

Research on finding the rotation center for non-circular gears, especially elliptical gears, is limited. This analysis aims to establish the rotation center by plotting the pitch curve based on formulas (16) and (17), determining as depicted in Fig. 5. The "long axis" is 48.17 mm, as shown by the red line, the "minor axis" is 46.82 mm, as shown by the blue line. Subsequently, the formula for calculating the focal length (see Fig. 5, O1-C1) of an ellipse is

$$c = \sqrt{a^2 - b^2} = \sqrt{(48.17/2)^2 - (46.82/2)^2}, \tag{19}$$

where a is the length of the semi-long axis, b is the length of the semi-minor axis, and c is the distance from the center of rotation to the center of the non-circular gear.

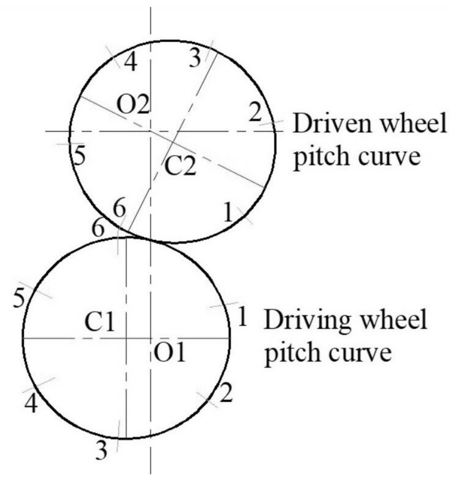

Fig. 5. The pitch curve of the non-circular gear

The c is calculated to be 5.66 mm, as shown in line O1-C1, O1 is the rotation center of the driving wheel. Similarly, the "focal length" of the driven gear and its rotation center O2-C2 is determined. The subsequent verification of the rotation center accuracy involves setting the tangent point as the initial reference and measuring six points of the same length (23.56 mm) to simulate pure rolling motion. The center distance, including the sum of O1-1 and O2-1, O1-2 and O2-2, etc. are documented. Results presented in Table 1, the sum of the six data points is very close to the center distance of 48.17 mm, with the maximum error noted as 0.13%, thereby validating the precision of the established rotation center. Figure 5 shows the initial rotation position.

Table 1
The distance from the rotation center to each point

Driving wheel	Length [mm]	Driven wheel	Length [mm]	Sum [mm]
O1-1	18.687	O2-1	29.417	48.104
O1-2	19.587	O2-2	28.524	48.111
O1-3	24.524	O2-3	23.651	48.175
O1-4	29.082	O2-4	19.140	48.222
O1-5	29.096	O2-5	19.101	48.197
O1-6	24.559	O2-6	23.558	48.117

Figure 6 expresses the mathematical model of the gear shaper cutter with a module of 2.5.

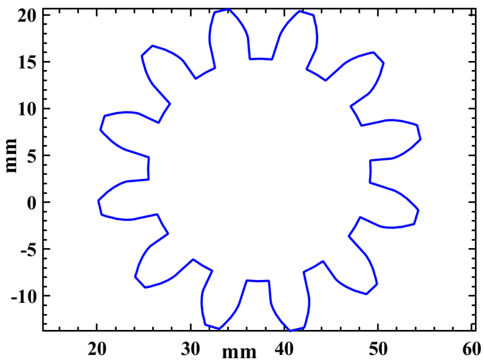

Fig. 6. Complete shape of a gear shaper cutter

3.3. Principles of shaping non-circular gear

The main modeling method for non-circular gear is the enveloping method, the cutter profile trajectory will envelop and form the profile of the non-circular gear during the machining process. Taking an external meshing gear [5] as an example, as shown in Fig. 7.

In Fig. 7, the dashed curve is the normal equidistant line of the pitch curve [5], which is also the trajectory of the gear shaper cutter center. A fixed coordinate system $O_0x_0y_0$ is established at the center of the non-circular gear. A moving coordinate system $O_Gx_Gy_G$ is established at the center of the inserter

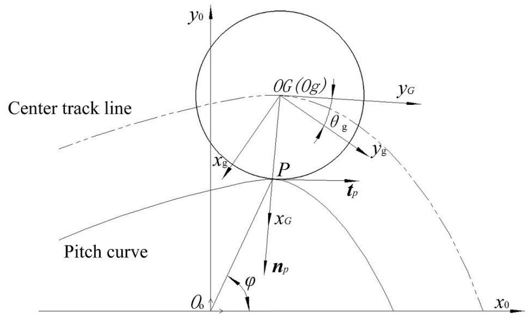

Fig. 7. External meshing non-circular gear

cutting tool. Since the inserter-cutting tool needs to move along the equidistant curve of the pitch curve and also rotate around the center O_G, a coordinate system $O_gx_gy_g$ fixed to the initial position of the inserter-cutting tool needs to be established on the coordinate system $O_Gx_Gy_G$.

The tooth profile of the non-circular gear [1] is the envelope of the tool tooth profile in the coordinate system $O_0x_0y_0$. To achieve this, it is necessary to determine the coordinate transformation matrix M_{1S} from the coordinate system $O_gx_gy_g$ to $O_Gx_Gy_G$, and the coordinate transformation matrix from the coordinate system $O_Gx_Gy_G$ to $O_0x_0y_0$.

M_{01} is obtained from the relationship of the non-circular gear pitch curve

$$M_{01} = \begin{bmatrix} -n_x & t_x & x_{n1} \\ -n_y & t_y & y_{n1} \\ 0 & 0 & 1 \end{bmatrix}. \tag{20}$$

The pitch curve of the non-circular gear is denoted as $r(\varphi_1)$, n_x and n_y are the components of the unit normal vector of the pitch curve, t_x and t_y are the components of the unit tangent vector of the pitch curve $r(\varphi_1)$, and x_{n1} and y_{n1} are the distance components between the origin of the coordinate system $O_0x_0y_0$ and $O_Gx_Gy_G$.

M_{1S} is obtained from the motion between the gear shaper cutter and the non-circular gear

$$M_{1S} = \begin{bmatrix} \cos\theta_g & -\sin\theta_g & 0 \\ \sin\theta_g & \cos\theta_g & 0 \\ 0 & 0 & 1 \end{bmatrix}. \tag{21}$$

The coordinate transformation matrix from $O_gx_gy_g$ to $O_0x_0y_0$ is M_{0s}, and $M_{0s} = M_{01}M_{1s}$.

The gear profile equation of the gear shaper cutter is given as $r_{01} = \begin{bmatrix} x_{01} & y_{01} & 1 \end{bmatrix}$, the envelope of the tool profile in the non-circular gear coordinate system can be obtained as

$$r_{K1}(\varphi_1) = M_{01}(\varphi_1)M_{1S}(\varphi_1)r_{01}. \tag{22}$$

Given the equation of the pitch curve and the gear shaper cutter parameters, the envelope diagram can be obtained, as shown in Figs. 10 and 11.

3.4. The enveloping method

In virtual machining, envelope interpolation of the gear stock is executed using the cutter model. The solution for non-circular gears primarily utilizes the enveloping method, which encompasses two primary approaches [15]: the equal polar angle method and the equal arc length method. From the consistency of tooth shape accuracy to consider, the equal arc length method proves superior for designing non-circular gear.

Using a numerical approach, the method divides the arc length uniformly to address the following transcendental equation

$$S = \int_{\varphi_1}^{\varphi_2} \sqrt{r^2 + (\mathrm{d}r/\mathrm{d}\varphi)^2}\,\mathrm{d}\varphi. \tag{23}$$

Formula (23) is a transcendental equation. Once the arc length of each segment is known, the polar diameter rotation angle corresponding to the length of the same arc length each turn S is inversely solved.

The outlined approach solves the polar diameter rotation angle corresponding to the length of the same arc length of each turn Swithout directly solving the transcendental equation (23).

1. Solving the pitch curve equation.
2. Utilizing formula (7) to derive the corresponding graph of polar diameter rotation angle versus arc length.
3. Determining the number of segments into which the arc length is divided and calculating the arc length for each turn S.
4. Using the data from Fig. 3, the rotation angle is inversely calculated according to the length of the same arc length each turn S.
5. Based on the obtained polar diameter rotation angle, employing the equal arc length method to generate a non-circular gears enveloping diagram.

The methodology is exemplified by analyzing the driving wheel, for which the calculated arc length is $L_1 = 149.2$ mm. The number of the same arc length sets 200 times, with the calculated length of the same arc length each turn is $S_1 = 0.746$ mm. Extensive data collection on the length of the same arc length each turn S_1 and corresponding to each polar diameter rotation angle, as evidenced in Table 2, which displays results from the first 20 iterations.

The non-circular gear enveloping diagrams are formed by the gear shaper cutter enveloping method, Figs. 8 and 9 show the relationship between the pitch curve, the gear shaper cutter, and the trajectory of the circular center of the cutter.

Table 2
The same arc length for each turn and the rotation angle of the driving gear

Arc length [mm]	Rotation angle [radian]	Arc length [mm]	Rotation angle [radian]
0.746	0.03205	8.206	0.36713
1.492	0.06436	8.952	0.40213
2.238	0.09692	9.698	0.43741
2.984	0.12975	10.444	0.47297
3.730	0.16285	11.190	0.50879
4.476	0.19622	11.936	0.54489
5.222	0.22985	12.682	0.58126
5.968	0.26376	13.428	0.61789
6.714	0.29794	14.174	0.65476
7.460	0.33239	14.920	0.69194

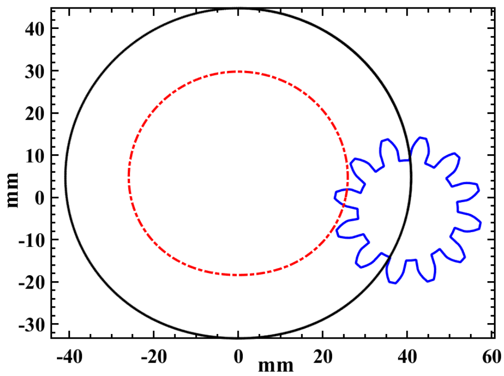

Fig. 9. The driven wheel pitch curve and shaper cutter

The enveloping diagrams for both driving and driven wheels are produced using the equal arc length enveloping method, these diagrams are displayed in Figs. 10 and 11.

Extracting tooth profile feature data requires solving the complex tooth surface meshing equation. To address this challenge,

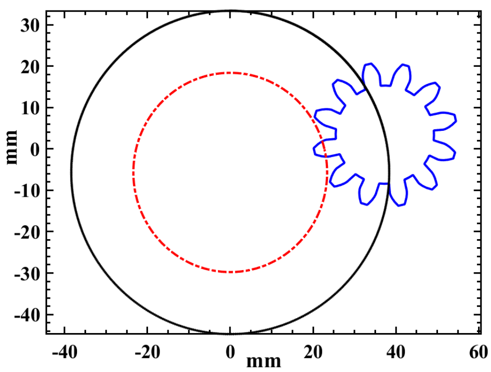

Fig. 8. The driving wheel pitch curve and shaper cutter

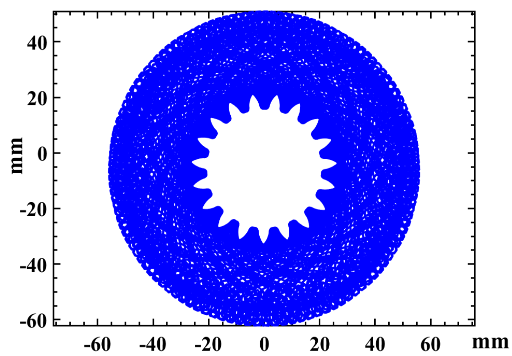

Fig. 10. Simulation result of driving gear machining with a shaper

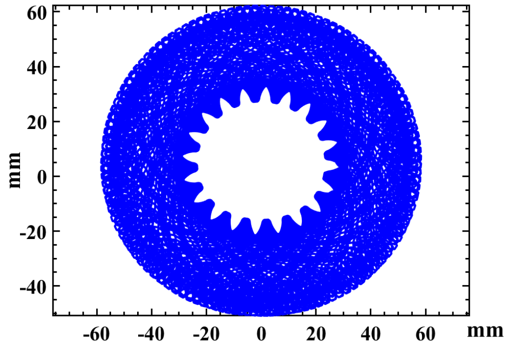

Fig. 11. Simulation result of driven gear machining with a shaper

(x_0-1, y_0+1)	(x_0, y_0+1)	(x_0+1, y_0+1)
(x_0-1, y_0)	(x_0, y_0)	(x_0+1, y_0)
(x_0-1, y_0-1)	(x_0, y_0-1)	(x_0+1, y_0-1)

(a) Eight neighboring positions

3	2	1
4	P	0
5	6	7

(b) Location coding

Fig. 13. Location and corresponding code

the paper integrates image processing technology and introduces an edge extraction algorithm that utilizes pixel extraction techniques to solve tooth profile feature points effectively.

4. EXTRACTION OF TOOTH PROFILE

4.1. Binary image processing

Upon obtaining the envelope diagram, it is saved as an image and subjected to a binarization process, as documented in references [16]. The results displayed in Fig. 12a and 12b indicate that the image comprises only two-pixel values: pure white is 1, and pure black is 0.

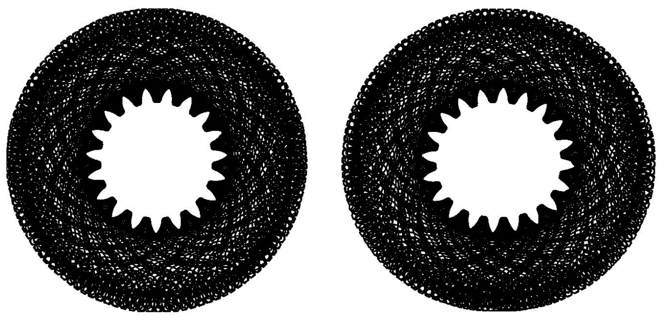

(a) Driving wheel (b) Driven wheel

Fig. 12. Binary image

4.2. Determine the starting point

The process begins by identifying the starting point. The method involves initiating from the central point of the binary image and scanning rightward until a black pixel is encountered [17], designated as (x_0, y_0). This point marks the commencement of the edge extraction algorithm.

4.3. The first search mechanism

Given that (x_0, y_0) is identified as an edge point, the next edge point [18] must be in the eight neighborhoods centered on (x_0, y_0), the coordinates are shown in Fig. 13a.

The search proceeds from the initial point (x_0, y_0), evaluating the surrounding pixels in a sequence dictated by Fig. 14. The search terminates upon encountering the first pixel is 0, indicating the location of the second edge point (x_1, y_1). Figure 14 is the first search approach.

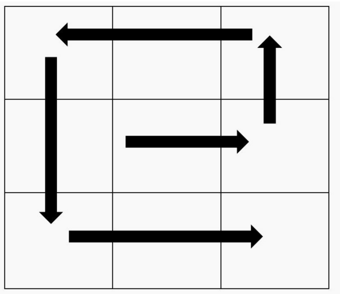

Fig. 14. The first search approach

4.4. Tracking criterion

Upon determining the initial point and obtaining point (x_1, y_1), subsequent boundary points must be in the eight neighborhood of point (x_1, y_1), which can be categorized into five cases.

Employing an edge extraction algorithm, as depicted in Fig. 15, allows for the inference of the next edge point direction based on the relative positions of previous and current points within their eight neighborhoods [19]. This algorithm efficiently computes the next edge point by examining up to five consecutive pixels in the predetermined edge direction, significantly reducing computational load compared to other edge extraction algorithms.

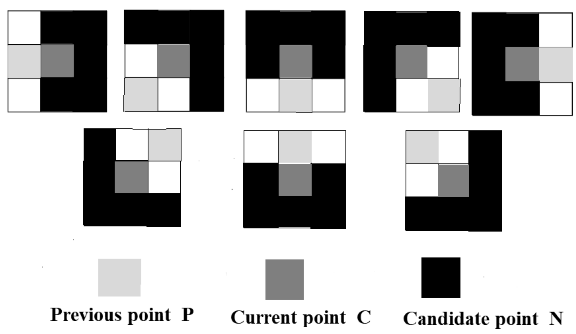

Fig. 15. The location relationship between the known point and candidate point

The method for locating the next edge point involves assuming current point C and previous point P are known, as shown in Fig. 15. Move two pixels clockwise from the location coding of point C relative to point P. If it is not an edge point, searching continues counterclockwise, conducting up to five searches to locate the next edge point. For example, if it is the first case in Fig. 15, as shown in Fig. 13b, move two pixels clockwise from location coding 0 to 7-6 sequentially; if location coding 6 is not the target point, then the search proceeds counterclockwise five times, the sequence 6-7-0-1-2. This intelligent memory remembers the previous position, you can search up to five times each time to find the next edge point, this intelligence reduces the time for subsequent searches.

The edge extraction algorithm presented in this paper and the method from Song [20] were used to perform edge extraction on Figs. 10 and 18a, with both images set to a DPI of 2100, resulting in the extraction of edge data through solving. The eight-neighborhood search using the method from Song [20] required 95 070 and 70 923 iterations for Fig. 10 and 18a, respectively. In contrast, using the algorithm in this paper only required 71 778 and 53 476 iterations for the 8-neighborhood search to complete the boundary extraction of the target object, improving efficiency by 24.5% and 24.6%, respectively. The algorithm in this paper demonstrates superior performance in extracting the target edge contours.

4.5. Overall flow of the algorithm

This process repeats as outlined in Section 4.4 until the loop closes upon rediscovery of the point (x_0, y_0). The edge extraction algorithm follows these steps:

1. Identify and set the starting point for pixel search and set it (x_0, y_0).
2. Conduct a counterclockwise search from the designated pixel to locate the first black pixel (x_1, y_1) in eight neighborhoods centered on (x_0, y_0).
3. If the point (x_1, y_1) is (x_0, y_0), go to step 5; or else, go to step 4.
4. Utilize the eight-neighborhood position and location coding of the previous point P and the current point C to determine the next direction of search and find a new edge point as the current point, then return to 3.
5. End of search.

4.6. Pixel to size conversion

Figure 16 depicts the relationship between pixel and actual size [20], allowing for the transformation of pixel coordinates (X, Y) into actual coordinates (x, y)

$$x = l_1 \times \frac{X}{n_1},$$
$$y = l_2 \times \frac{Y}{n_2}. \tag{24}$$

The real dimensions of the extracted tooth profile are calculated using formula (24), and the real size is obtained, as shown in Fig. 17a and 17b.

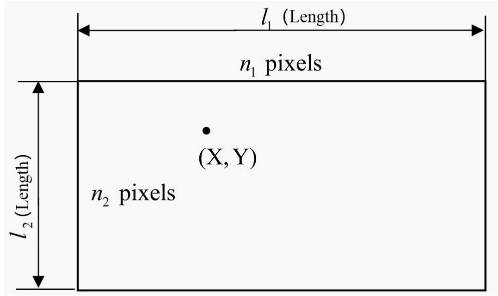

Fig. 16. The actual size and pixel size

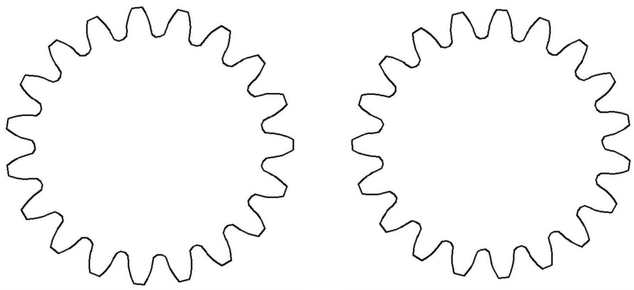

(a) Driving gear (b) Driven gear

Fig. 17. The actual size of the driving and driven gear

4.7. Precision analysis

The edge extraction algorithm precision is evaluated by extracting the edge of the circle, aiming to determine the accuracy of the method [20]. As shown in Fig. 18a, the length of the black square is 30 mm, and the circle radius is set at 10 mm. Figure 18b is the circle extracted using the edge extraction algorithm proposed in this paper.

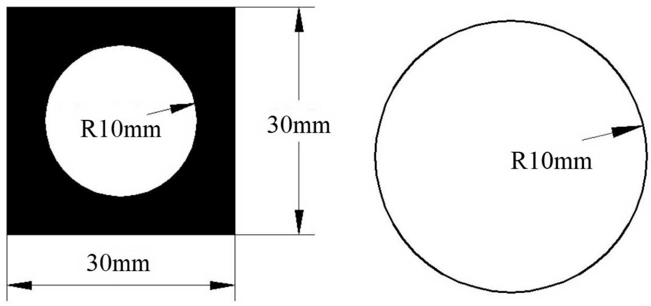

(a) (b)

Fig. 18. A square and an extracted circle

Set different picture quality as variable, by changing the DPI (dots per inch) of the picture in Fig. 18a, as shown in Table 3. When DPI is 300, 900, 1500, and 2100, respectively, the average errors are 0.537%, 0.179%, 0.111%, and 0.081%. These results affirm that the edge extraction algorithm has high precision in extracting edge point data from pictures. The accuracy and high precision of the tooth profile extraction algorithm in this study have been verified. This article uses the picture with a DPI of 2100 for comprehensive analyses.

Table 3
Different picture quality and radius range of the extracted circle

Picture DPI	300	900	1500	2100
Maximum deviation [mm]	0.03959	0.03033	0.02779	0.02678
Radius fluctuation range [mm]	0.05371	0.01793	0.01112	0.00811

4.8. Comparison of methods

This paper compares the tooth profile extraction algorithm for non-circular gears used in this study with those found in the existing literature (Wang [5]). Taking the driving gear in this study as the research object (as shown in Fig. 10), tooth profile points are extracted using two methods. The comparison data is presented in Table 4.

Table 4
The results of the different methods

Comparison item	Xuan Wang's method [5]	This paper method
Number of tooth profile points	About 608	About 17 000
Time spent	More than 2 hours	Less than 20 seconds
Missing part of tooth profile point	Tooth top, tooth root	None
Programming difficulty	Difficulty	Easy

Compared with other tooth profile extraction algorithms, the proposed algorithm has the advantages of fast operation speed, high integrity of tooth profile extraction, simple programming, and ease of understanding.

5. KINEMATICS ANALYSIS

5.1. Non-circular gear assembly

Import the extracted tooth profile data into Pro/E software, where it undergoes a stretching process with a specified thickness of 40 mm. After stretching, the gear 3D model includes a centrally located 6 mm hole, set as the assembly position based on the rotation center obtained in Fig. 5, as shown in Fig. 19.

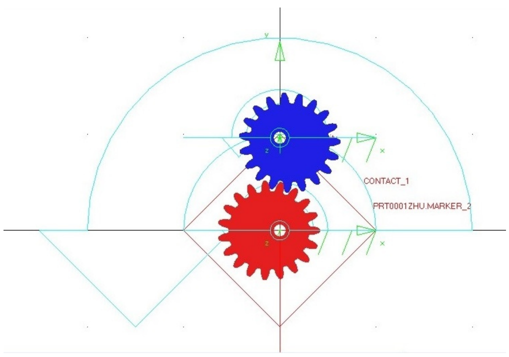

Fig. 19. Assembly drawing in ADAMS

5.2. Parameter setting

Using ADAMS software, a kinematic analysis [21] of a non-circular gear pair is conducted. In ADAMS software, density is $7.8 \cdot 10^{-6}$ kg/mm^3, Young's modulus is $2.07 \cdot 10^5$ N/mm^2, and Poisson's ratio is 0.29. A contact force constraint is applied, simulating the interaction between two rigid bodies allowed to penetrate slightly. The stiffness of the material is 2000 N/mm, with a force index of 2.2, and the maximum damping is 400 Ns/mm. The rotation center is configured as a rotating pair, and the rotational drive is activated at the driving wheel rotation center, as depicted in Fig. 19. This setup drives the rotation at 30 degrees per second, the duration of exercise is 32 seconds, and the number of steps is 320. Figure 20 illustrates the angular speeds of the driven wheel.

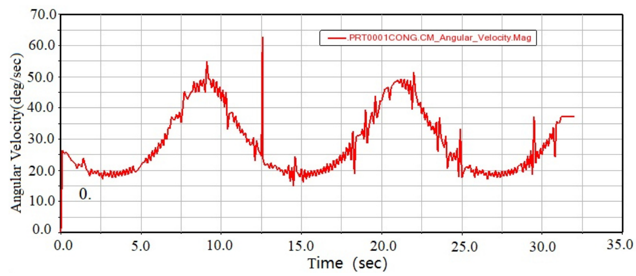

Fig. 20. Driven wheel angular speed

This observation, as demonstrated in Fig. 20, where the angular speed response curve of the driven wheel displays noticeable fluctuations. Due to irregular vibration excitation from continuous changes in contact ratio during meshing. These observations confirm the actual operational consistency of non-circular gears. By analyzing Fig. 20 and the target transmission ratio, it can be concluded that the angular velocity curve of the driven wheel obtained from Adams is consistent with the target transmission ratio, proving that the design meets the requirements of the target transmission ratio.

5.3. Numerical calculation

Figure 21 illustrates the meshing diagram of the non-circular gear pair, with each tooth numbered and distances from the

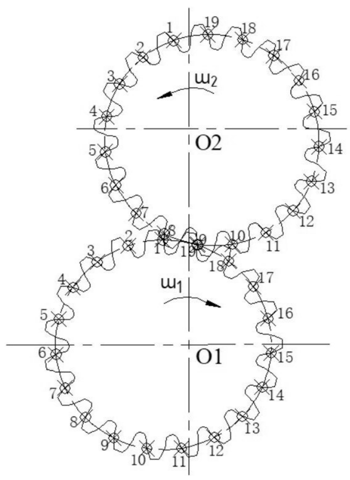

Fig. 21. Designed non-circular gear pair

rotation center to each tooth quantified [7], as detailed in Table 5. The angular speed of the driving gear is set at 30 degrees per second, to simplify the table, therefore, only select tooth data are displayed. Note: the angular speed unit is degrees per second. The non-circular gear pair transmission ratios and the rotation angles of the driving wheel in Table 5 are shown in Fig. 22, and the angular speed of the driven wheel and the rotation angles of the driving wheel are presented in Fig. 23.

Table 5
Numerical calculation of the non-circular gear

Meshing teeth input-output	Driving wheel [mm]	Driven wheel [mm]	Driving wheel rotation angle [°]	Transmission ratio	Driven wheel angular speed
1-8	24.103	24.041	14	0.997	30.077
3-6	27.564	20.593	48	0.747	40.155
5-4	29.600	18.573	79	0.627	47.811
7-2	29.279	18.913	109	0.646	46.443
9-19	26.749	21.444	141	0.802	37.422
11-17	23.139	25.041	176	1.082	27.721
13-15	19.921	28.263	217	1.418	21.145
15-13	18.421	29.755	264	1.615	18.573
17-11	19.358	28.805	312	1.488	20.161
19-9	22.284	25.875	355	1.161	25.837

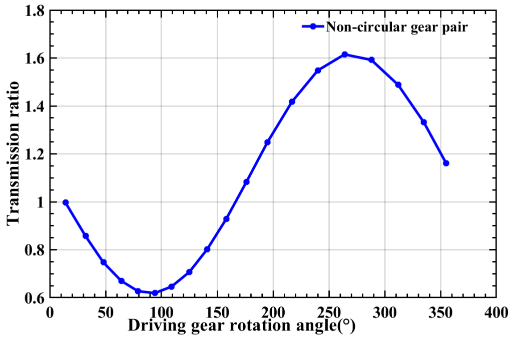

Fig. 22. Non-circular gear transmission ratio

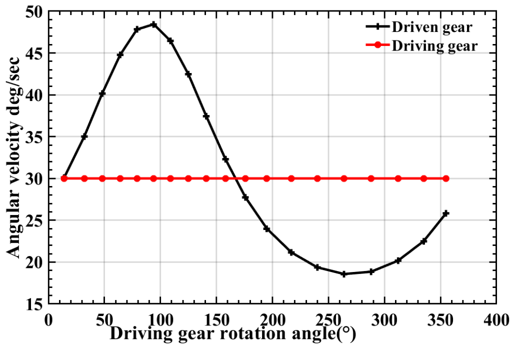

Fig. 23. Rotation angle and angular speed

The analysis of the results in Fig. 22 compares them to the transmission ratio $i_{12}(\varphi_1) = 1.118 + 0.5\sin(\varphi_1)$ and shows that the two diagrams are the same. Further examination of Fig. 23 and Fig. 20 corroborates that the calculated angular speed curve aligns with the value obtained by ADAMS software simulation, affirming the validity of the design methodology.

6. EXPERIMENTAL VERIFICATION

6.1. Non-circular gear manufacturing

Non-circular gears are fabricated using CNC wire-cut electric discharge machining, achieving a machining precision ≤ 0.005 mm. The material is a 65 Mn hot-rolled steel plate with a 10 mm thickness. Figure 24a showcases these details, and Fig. 24b shows the result, with a center distance of 48.17 mm. The gear pair rotates flexibly without any obstruction, demonstrating that the designed tooth profiles are reasonable. Experimental results validate the accuracy of this method.

(a) (b)

Fig. 24. Wire-cut machining of non-circular gears

6.2. Non-circular gear detection

To verify the accuracy of the non-circular gears produced using the tooth profile data obtained by the algorithm in this paper, an Edwards DH3020 imaging measurement machine was used to measure the non-circular gears, with an accuracy of $(3.0 + L/200)$ µm. The process of detecting non-circular gears with an imaging measurement machine is shown in Fig. 25.

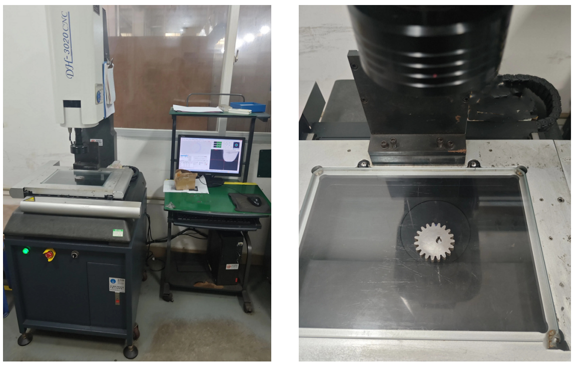

Fig. 25. Imaging measurement machine measuring non-circular gear

The measured tooth profile data are compared with the edge data of the envelope image. Taking the driving gear as the research object, two teeth are selected for analysis. Only a part of the data on the tooth profile is chosen for analysis, including the nodes where the pitch curve intersects the tooth profile, the tooth top points, and the tooth root points. By comparing the five measured coordinate positions obtained from the imaging measurement machine with the coordinates in the enveloping image, the distance between the coordinates at each node can be determined. Figure 26 displays the locally magnified view.

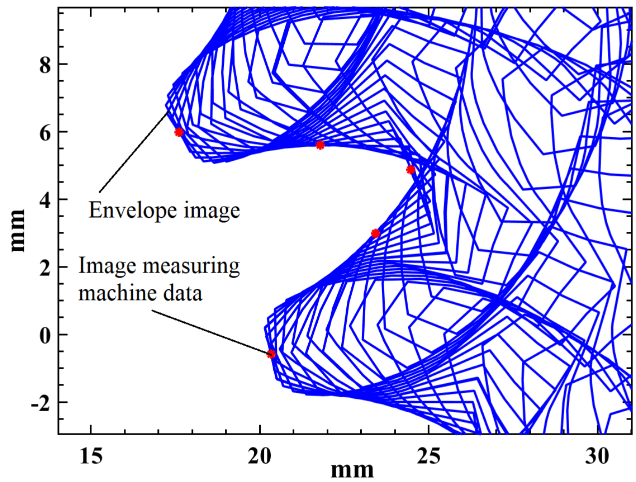

Fig. 26. Partially magnified view of the envelope image

For the driven gear, two teeth are selected using the same method, and the selected coordinate points are sequentially labeled, as shown in Fig. 27. The results are presented in Table 6, and the lengths in Table 6 represent the distances between the data from the imaging measurement machine and the enveloping image data.

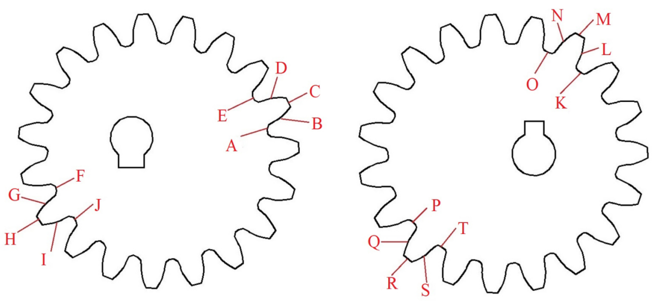

Fig. 27. Non-circular gear tooth profile analysis positions

As shown in Table 6, based on the error distribution results from reference [19], the measurement distances between the coordinate points detected by the imaging measurement machine and the coordinates of the profile nodes in the enveloping image are reasonable. The actual tooth profile matches the theoretical tooth profile, which proves that the results of the actual wire-cutting process for non-circular gear are correct.

Table 6
The length between the points measured by the image-measuring machine and the envelope image

Position	Length/mm	Position	Length/mm
A	0.0276	K	0.0315
B	0.0324	L	0.0359
C	0.0287	M	0.0198
D	0.0349	N	0.0276
E	0.0413	O	0.0392
F	0.0194	P	0.0377
G	0.0231	Q	0.0418
H	0.0313	R	0.0181
I	0.0358	S	0.0340
J	0.0396	T	0.0427

7. CONCLUSIONS

This paper puts forward a design method for non-circular gears grounded in specific transmission ratios. The envelope image is generated using the equal arc length enveloping method, then an edge extraction algorithm is applied to extract the tooth profile. Kinematic analysis and non-circular gear detection are performed to validate the design. The conclusions are as follows.

1. Equal arc length algorithm: This paper presents an equal arc length interpolation algorithm that avoids the need to solve transcendental equations. This algorithm offers several benefits, including less computation, ease of programming, and simplicity in the solving process.
2. Edge extraction algorithm: This method addresses the extraction of non-circular gear tooth profiles, circumventing the need to solve complex gear meshing equations. Key advantages of this algorithm include precise tooth profile extraction, elimination of intricate numerical calculation, ease of understanding, and high solving speed.
3. Kinematic analysis: The results are closely aligned with the target transmission ratio. This confirms the feasibility of the proposed design method, which can tailor non-circular gear pairs to specific transmission ratios and varied pitch curve equations. Subsequently, contact characteristic analysis, CNC machining, and manufacturing can be conducted.
4. Non-circular gear inspection: The measurement deviation between machined tooth profile node coordinates and theoretical tooth profile node coordinates is within a reasonable range, meeting the design requirements. The actual tooth profile is consistent with the theoretical tooth profile.
5. Applicability of the edge extraction algorithm: The edge extraction algorithm is capable of extracting tooth profiles from non-circular gears shaped by gear shaper cutters and hobbing cutters, demonstrating broader applicability compared to other tooth profile-solving algorithms.

REFERENCES

[1] Y. Liu, L. Wu, and C. Dong, "Investigation of contact ratio and dynamic characteristics of non-circular planetary gear train in hydraulic motor," *Flow Meas. Instrum.*, vol. 100, pp. 1–14, 2024, doi: 10.1016/j.flowmeasinst.2024.102720.

[2] J.J. Yang, M.L. Zhou, D.Q. Yin and J.J. Yin, "Design and Development of Rice Pot-Seedling Transplanting Machinery Based on a Non-Circular Gear Mechanism," *Appl. Sci.-Basel.*, vol. 14, no. 3, pp. 1027, 2024, doi: 10.3390/app14031027.

[3] J. Dai, S. Wang, D. Zhang, B. Zi, G. Cui, and H. Ding, "Error Detection and Classification of Tangential Radial Single Machining of Non-Circular Gear," in Proc. *3rd International Conference on Mechanics and Mechatronics Research.*, 2016, pp. 01032–01032, doi: 10.1051/matecconf/20167701032.

[4] Y. Liu, X. Ren, and C. Dong, "Transmission performance analysis of non-circular gear hydraulic motor," *Jordan J. Mech. Ind. Eng.*, vol. 18, no. 3, pp. 635–644, 2024, doi: 10.59038/jjmie/180316.

[5] X. Wang, "A numerical algorithm of tooth profile of non-circular cylindrical gear," in Proc. *5th International Conference on Information Science, Automation and Material System. (ISAM)*, 2017, pp. 020174–020174, doi: 10.1063/1.4992991.

[6] HS. Jang, HL. Chang, GY. Park, and C. Kim "Study on Design of Non-Circular Gears for Speed Control of the Squid Belly Opening and Gutting Machine (SBOGM)," *Appl. Sci.*, vol. 3268, no. 11, pp. 2–15, 2021, doi: 10.3390/app11073268.

[7] S. Maláková, M. Urbansky, G. Fedorko, and S. Sivak, "Design of Geometrical Parameters and Kinematical Characteristics of a Non-Circular Gear Transmission for Given Parameters," *Appl. Sci.*, vol. 1000, no. 11, pp. 2–24, 2021, doi: 10.3390/app11031000.

[8] D. Liu and T. Ren, "Study on Deformed Limacon Gear and Motion Optimization of its Serial Mechanism," *J. Mech. Des.*, vol. 133, no. 6, p. 061004, 2011, doi: 10.1115/1.4004116.

[9] G. Figliolini, "Synthesis of the base curves of non-circular gears via the return circle," *Adv. Manuf.*, vol. 28, pp. 540–550, 2014, doi: 10.1533/9781782421955.540.

[10] Y.Y. Liu and J.S. Diao, "Six-Axis Linkage Strategy and Its Models for Non-Circular Helical Gears Based on Diagonal Hobbing," *Strojniski Vestn.-J. Mech. Eng.*, vol. 61, no. 5, pp. 330–340, 2015, doi: 10.5545/sv-jme.2014.2371.

[11] J. He *et al.*, "Study on Minimum Teeth without Undercutting of Standard Involute Gears," *Adv. Mater. Res.*, vol. 199, pp. 329–336, 2011, doi: 10.4028/www.scientific.net/KEM.544.497.

[12] A.A. Prikhod'Ko and A.I. Smelyagin, "Kinematics of a Planetary Train with Elliptical Gears with Internal Gearing," *J. Mach. Manuf. Reliab.*, vol. 50, no. 5, pp. 412–418, 2021, doi: 10.3103/S1052618821050095.

[13] S. Medvecká-Beňová, "Meshing Condition and Kinematic Properties of non-circular Gear," *Acta Mech. Slovaca*, vol. 20, no. 2, pp. 16–21, 2016, doi: 10.21496/AMS.2016.010.

[14] F.Y. Zheng, L. Hu, X.H. Han, B. Li, and D.F. Chen, "Linkage model and manufacturing process of shaping non-circular gears," *Mech Mach Theory,* vol. 96, pp. 192–212, 2016, doi: 10.1016/j.mechmachtheory.2015.09.010.

[15] M. Xu, X.H. Han, L. Hua and F.Y. Zheng, "Modeling and methods for gear shaping process and cutting force prediction of variable transmission ratio rack," *Int. J. Mech. Sci.*, vol. 171, p. 105364, 2020, doi: 10.1016/j.ijmecsci.2019.105364.

[16] J. Yao, Y.B. Xue, X.L. Li, L. Zhai, Z.Y. Yang and W.H. Zhang, "Machine Vision Online Detection of Ore Granularity Based On Edge Computing," *Arch. Min. Sci.*, vol. 68, no. 2, pp. 335–350, 2023, doi: 10.24425/ams.2023.146183.

[17] C. Orhei, V. Bogdan and C. Bonchis, "Dilated filters for edge detection algorithms," *Appl. Sci.*, vol. 11, no. 22, p. 10716, 2021, doi: 10.3390/APP112210716.

[18] B.Z. Wei and Z.M. Zhao, "A sub-pixel edge detection algorithm based on Zernike moments," *Imaging Sci. J.*, vol. 61, no. 5, pp. 436–446, 2013, doi: 10.1179/1743131X12Y.0000000024.

[19] G.Z. Zhang, J. Han and Y.Y. Liu, "Gear hobbing machining method and its principle for higher order elliptic gears," *Comput. Integr. Manuf. Syst.*, vol. 20, no. 5, pp. 1106–1113, 2014, doi: 10.13196/j.cims.2014.05.zhangguozheng.1106.8.20140513.

[20] W.Z. Song, Y.He and Y.H. Zhou, "Design and extraction of tooth profile of denatured elliptical gear," *Adv. Mech. Eng.*, vol. 14, no. 12, pp. 1–12, 2022, doi: 10.1177/16878132221144544.

[21] K.H. Zhou, M.L. Xi, Y.T. Guo and X. Lu, "Simulation Research on Non-Bevel Gear Transmission Mechanism," *Mechanika.*, vol. 29, no. 6, pp. 502–510, 2023, doi: 10.5755/j02.mech.33584.